Geometry-Based Models for Studying the Effects of Wind Farm Layout

NIRANJAN S. GHAISAS AND CRISTINA L. ARCHER

College of Earth, Ocean, and Environment, University of Delaware, Newark, Delaware

(Manuscript received 13 October 2014, in final form 30 April 2015)

ABSTRACT

Layout studies are critical in designing large wind farms, since wake effects can lead to significant reductions in power generation. Optimizing wind farm layout using computational fluid dynamics is practically unfeasible today because of their enormous computational requirements. Simple statistical models, based on geometric quantities associated with the wind farm layout, are therefore attractive because they are less demanding computationally. Results of large-eddy simulations of the Lillgrund (Sweden) offshore wind farm are used here to calibrate such geometry-based models. Several geometric quantities (e.g., blockage ratio, defined as the fraction of the swept area of a wind turbine that is blocked by upstream turbines) and their linear combinations are found to correlate very well (correlation coefficient of ~0.95) with the power generated by the turbines. Linear models based on these geometric quantities are accurate at predicting the farm-averaged power and are therefore used here to study layout effects in large wind farms. The layout parameters that are considered include angle between rows and columns, angle between incoming wind and columns (orientation), turbine spacings, and staggering of alternate rows. Each can impact wind power production positively or negatively, and their interplay is complex. The orientation angle is the most critical parameter influencing wake losses, as small changes in it can cause sharp variations in power. In general, for a prevailing wind direction, the orientation angle should be small (7.5°–20°) but not zero; staggering and spacing are beneficial; and nonorthogonal layouts may outperform orthogonal ones. This study demonstrates the utility of simple, inexpensive, and reasonably accurate geometry-based models to identify general principles governing optimal wind farm layout.

1. Introduction

Interactions among the wakes of individual turbines in a large wind farm have a significant impact on the overall performance of the wind farm. Depending on the wind direction and the layout of the turbines, the actual power produced can be significantly lower than the rated power of the wind farm (Archer et al. 2013; Wu and Porté-Agel 2013; Stevens et al. 2014). Optimal layout of wind turbines is, therefore, a crucial element in modern wind farm design considerations.

A variety of numerical and analytical techniques have been developed over the years to study wind turbine wakes. Computational fluid dynamics (CFD) studies of wind farms can be classified based on the type of turbulence closures employed. Studies such as Barthelmie et al. (2009) and Tian et al. (2014) use the Reynolds-averaged Navier–Stokes (RANS) approach for modeling the effect of turbulence. Numerical tools such as the Universidad Politécnica de Madrid version of the Park model (UPMPARK), the Technical University of Denmark "EllipSys" solver, and the Risø National Laboratory "Fuga" model (Archer et al. 2014) are all based on the RANS turbulence modeling approach. RANS simulations are not suitable for resolving the details of the unsteady features of turbulent flows, which are better captured by the large-eddy simulation (LES) technique (Churchfield et al. 2012a; Calaf et al. 2010, 2011; Stevens et al. 2014; Archer et al. 2013).

A number of studies have focused on evaluating the effects of wind farm layout on power generation. Meyers and Meneveau (2012) determined the optimal spacing in infinitely large wind farms, where the turbines were arranged in rows perfectly aligned with the incoming wind direction. The optimal spacing, assumed equal in the streamwise and spanwise directions, was found to be much larger than the spacing typically used in existing wind farms. The effect of staggering was studied by Wu and Porté-Agel (2013) in a downscaled wind farm

Corresponding author address: Cristina L. Archer, College of Earth, Ocean, and Environment, University of Delaware, 111 Robinson Hall, Newark, DE 19716.
E-mail: carcher@udel.edu

DOI: 10.1175/JTECH-D-14-00199.1

© 2016 American Meteorological Society

comprising 30 miniature turbines. Staggering alternate rows was found to increase the angular speed of the turbines because of exposure to higher local wind speeds. Stevens et al. (2014) studied the alignment of rows of turbines in infinitely large wind farms with the wind direction. They found that the configuration with rows aligned at a small angle to the incoming wind yielded the maximum power. The optimal angle was smaller than the angle corresponding to perfect staggering of rows and was dependent on the turbine spacing in the spanwise direction. None of the above studies were carried out on actual wind farms, and most of them considered infinitely large wind farms, a necessary assumption for applying periodic conditions in the horizontal directions. A numerical investigation of layout effects in an actual, finite, wind farm offshore of Lillgrund (Sweden) was carried out by Archer et al. (2013). A number of layouts, generated by staggering rows, increasing streamwise and/or spanwise spacings, and simultaneously staggering and increasing spacings, were evaluated. Wind farm layouts were shown to affect the performance by up to 33%.

While useful in identifying certain features of layout effects, the above studies are limited in the combinations of layout design parameters and the number of layouts that can be evaluated. This is because CFD simulations, especially LES of large wind farms, are extremely computationally demanding. For example, each simulation of the Lillgrund wind farm reported in Archer et al. (2013) required on the order of 150 000 CPU hours. A simple and inexpensive method of investigating the effects of wind farm layout is needed, and this has motivated development of several analytical models.

Analytical models that are easy to implement and practical to use for layout studies follow from either the classical Park model (Jensen 1983; Katic et al. 1986; Peña et al. 2013a,b; Bastankhah and Porté-Agel 2014; Nygaard 2014) or the so-called top-down approach (Frandsen 1992; Emeis and Frandsen 1993; Frandsen et al. 2006; Calaf et al. 2010; Meyers and Meneveau 2012). The Park family of models accounts for lateral spread of wind turbine wakes and is able to account for the effects of turbine layout (Katic et al. 1986). However, these models ignore the vertical structure of the atmospheric boundary layer (ABL) and the interactions between wind turbine wakes and the ABL. The top-down models, on the other hand, are able to account for the ABL vertical characteristics on the wind farm performance by assuming the presence of two constant-stress regions above and below the wind turbine rotors (Calaf et al. 2010). These models depend only on the mean spacing between turbines and consequently do not account for the details of the horizontal layout of turbines. This assumption is justified in the fully developed regime, applicable to infinitely large arrays of wind turbines (Emeis and Frandsen 1993). Extensions of the top-down model to account for entrance effects in finite wind farms have been carried out by Meneveau (2012). Models coupling the above two contrasting approaches have been developed (Frandsen et al. 2006; Stevens et al. 2015), as have also models accounting for the effects of atmospheric stability (Emeis 2010; Peña et al. 2013a,b; Peña and Rathmann 2014).

All of the abovementioned analytical models use the principle of momentum conservation to predict the wake velocity, which is then coupled to a power curve to determine the generated power. Thus, these models attempt to take into account the physical processes occurring during turbine wake interactions and hence may be termed ''physics based'' models. In contrast, in the current study, an attempt is made to develop simple statistical models that rely only on the geometry of the wind farm to directly predict the generated power. Several geometric features associated with a given wind farm layout are defined in section 2. A series of LES of the Lillgrund wind farm, which are reported elsewhere (Archer et al. 2013), are used to calibrate models based on some of these geometric features. The models are validated in section 3 by their ability to reproduce the Lillgrund LES and other numerical simulation results, and difficulties in comparing with field observations are pointed out. The models are employed to study the effects of wind farm layout in hypothetical configurations in section 4. A number of design features, such as the streamwise and spanwise spacings, the staggering of alternate rows, the angle between the rows and the columns, and the wind farm orientation are varied. Some general conclusions regarding wind farm layout are drawn. Section 5 presents the summary and conclusions of this study demonstrating the utility of such geometry-based models in analyzing wind farm layout effects, as well as their limitations.

2. Geometry-based models

a. *Overview of LES results*

The Lillgrund wind farm, located off the coast of Sweden in the Baltic Sea, has 48 wind turbines (Siemens; 2.3 MW with diameter $D = 93$ m and hub height of 63.4 m) arranged in an exceptionally tight (close spaced) layout (Dahlberg 2009). This tight spacing makes this farm site ideal for studying the effects of different layouts, such as varying the spacing between turbines along (streamwise) and across (spanwise) a given wind direction. The wind turbines in Lillgrund are represented

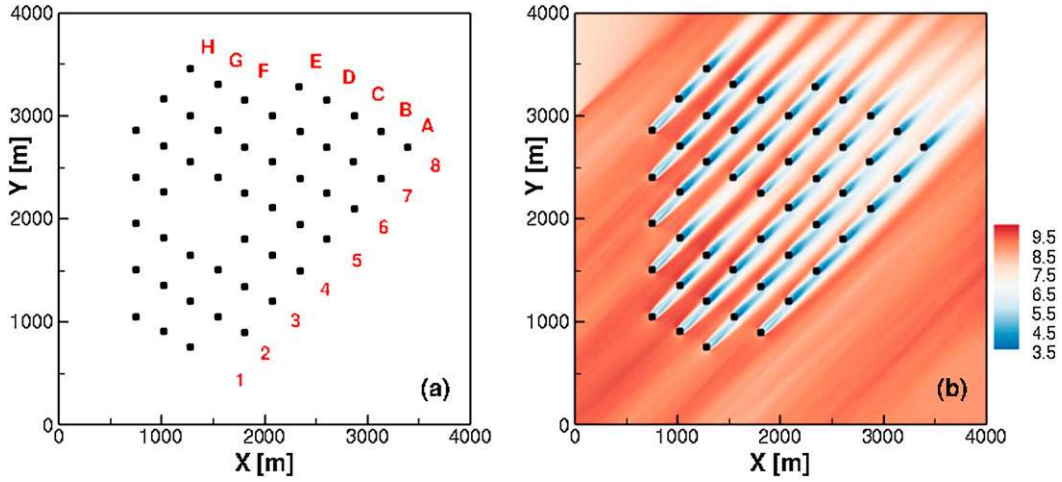

FIG. 1. (a) Layout of turbines in the Lillgrund wind farm. Filled circles denote the wind turbines, rows are numbered 1–8, and columns are lettered A–H. (b) Time-averaged horizontal velocity ($m\,s^{-1}$) contours at the vertical level $Z = 90$ m, obtained from LES of the Lillgrund wind farm under neutral stability and wind coming from 225° (southwest).

by solid circles in Fig. 1a. A number of large-eddy simulations of the Lillgrund wind farm, with the turbine blades represented as rotating actuator lines, were carried out, as described in Archer et al. (2013), and are summarized in Table 1. For each case, the number of turbines, the wind direction, a brief description of the layout, and the total power generated P_{TOT} are listed. Also included is the averaged relative power, defined as

$$P_{\mathrm{rel}} = \frac{\sum_{i=1}^{N_T} P_i}{N_T P_{\mathrm{max}}}, \tag{1}$$

where P_i denotes the power generated by the ith turbine, N_T denotes the number of turbines, and P_{max} denotes the maximum power among the N_T turbines (generally produced in the first upstream row of turbines). As shown in Table 1, the simulations include wind blowing from the southwest (marked 225), west (270), and northwest (315). The prevailing wind direction, or the direction from which the wind blows most often, is southwest at Lillgrund (Bergström 2009). With the same southwesterly wind, simulations of five additional layouts were carried out, with double the spacing in the streamwise (Spa-L), spanwise (Spa-X), and both (Spa) directions, with a staggered (Stag) layout and a staggered layout with double the spacing in both directions (Stag-Spa). All eight simulations were carried out under neutral atmospheric conditions, with a fixed wind speed of $9\,m\,s^{-1}$ at 90 m. Because of vertical wind shear, this meant a wind speed of $8.7\,m\,s^{-1}$ at hub height. All simulations had an incoming turbulent inflow with a turbulence intensity (TI) of approximately 7.3% at hub height.

The Simulator for Wind Farm Applications (SOWFA), developed by the National Renewable Energy Laboratory, was used for these simulations. SOWFA uses the Open Source Field Operation and Manipulation (OpenFOAM; http://www.openfoam.org/index.php) computer-software toolbox to solve the incompressible

TABLE 1. Summary of LES results for the Lillgrund wind farm with neutral stability. Wind direction is in degrees from north, and P_{TOT} is in megawatts.

Label	Wind direction	Layout	N_T	P_{TOT}	P_{rel}
225	225	Original	48	33.4	0.695
270	270	Original	48	32.4	0.675
315	315	Original	48	43.3	0.903
Stag	225	Alternate rows staggered	48	37.9	0.789
Stag-Spa	225	Staggered, double spacing in both directions	26	24.2	0.929
Spa	225	Original, double spacing in both directions	12	10.6	0.885
Spa-X	225	Original, double spacing spanwise	23	15.9	0.692
Spa-L	225	Original, double spacing streamwise	25	22.2	0.886

Navier–Stokes equations. The equations were discretized using a finite-volume framework with collocated storage of variables and second-order accuracy in space and time. For these neutrally stratified simulations, the subgrid-scale stresses were computed using the classical Smagorinsky (Smagorinsky 1963) model. The simulations included precursor computations without wind turbines for generating a turbulent atmospheric boundary layer, followed by wind plant computations with wind turbines included. SOWFA has been previously validated for its ability to set up a turbulent atmospheric boundary layer in the absence of wind turbines (Churchfield et al. 2012a) and for its reasonable accuracy in simulating the Lillgrund wind farm (Churchfield et al. 2012b).

Of a total of eight simulations listed in Table 1, details regarding six simulations with a southwesterly wind are described in Archer et al. (2013). As an example of the LES results, the time-averaged horizontal velocity field obtained from the control case (i.e., original layout) is shown in Fig. 1b. The results of these eight LES are used here to formulate statistical models based on geometric measures, defined next.

b. Geometric measures in wind farms

We assume a wind farm comprising N_T turbines located over flat terrain or over water. The domain is assumed to be a rectangular box, with the Cartesian X and Y axes aligned in the horizontal plane, along the east–west and north–south directions, respectively. The Z axis is aligned vertically. All turbines have identical hub heights Z_h and rotor diameters D. The corresponding area swept by the rotor blades (swept area) is also identically equal to $A = \pi D^2/4$. The farm layout is simply a list of the X and Y coordinates of each turbine i. Following the meteorological convention, the wind direction is described by the angle θ, varying from 0° to 360°, that it makes with the north, clockwise. It is further assumed that the nacelle yaw angles change with θ in such a way that the turbine swept areas are always perfectly normal to the wind.

Given a layout and a wind direction, a number of purely geometric quantities can be defined for each turbine. Five quantities, which can potentially be useful in modeling the power generated by the wind farm, are defined below. For any such measure Q_i defined for an individual turbine i, the corresponding farm-averaged quantity can also be defined as $Q = N_T^{-1}\sum_{i=1}^{N_T} Q_i$.

The first quantity is *blockage ratio* BR_i, defined as the fraction of the swept area of turbine i that is blocked by the swept area of *any* upstream turbine, for a given wind direction. Each turbine is assumed to influence (and be influenced by) only turbines within the cylinder with cross section equal to the swept area and aligned along the wind direction. There may be multiple upstream turbines that block the same or additional portions of the swept area of a given turbine. The BR_i is a ratio, varying over the set [0, 1], that is determined by an integral over the swept area of the turbine as follows:

$$\mathrm{BR}_i = \frac{1}{A}\int_{(x,y)\in A} \chi \, dx \, dy, \tag{2}$$

where $\chi = \chi(x, y)$ is defined for each point (x, y) on the turbine rotor disk and is equal to 1 if point (x, y) is blocked by any upstream turbine and is zero otherwise. Note that χ is a discontinuous function defined for every point (x, y) on the turbine rotor disk, whereas BR_i is associated with the entire turbine swept area.

The second quantity is *blockage distance* BD_i and is given by the equation

$$\mathrm{BD}_i = \frac{1}{A}\int_{(x,y)\in A} [L\chi + (1-\chi)L_\infty] \, dx \, dy, \tag{3}$$

where χ is as defined above. Similar to χ, $L = L(x, y)$ is a function of every point (x, y) on the turbine rotor disk and denotes the distance to the upstream blocking turbine. Wherever $\chi = 0$, that point on the swept area of turbine i is not blocked by any other turbine swept area and L is infinite. Term L_∞ is an arbitrary large, but finite, length that is introduced to ensure that the integral remains finite. In this study, we set $L_\infty = 20D$ since previous studies (Xie and Archer 2015; Wu and Porté-Agel 2011) have shown that the velocity profile in a turbine wake almost entirely recovers its original shape by $20D$ downstream of the turbine. The blockage distance may be thought of as an average of the distances to the upstream blocking turbines, weighted by the fraction of the area blocked by each upstream blocking turbine. The BD_i is therefore not entirely independent of BR_i because BD_i and BR_i are functions of χ. The BD_i can be normalized by dividing it by L_∞.

The third quantity, *inverse blockage distance* IBD_i, is similar to the blockage distance except that the reciprocal of the distance is used in place of the distance to the blocking turbine:

$$\mathrm{IBD}_i = \frac{1}{A}\int_{(x,y)\in A} \frac{1}{L}\chi \, dx \, dy. \tag{4}$$

Since the reciprocal of the distance L is used, no arbitrary large value needs to be introduced for points on the swept area of turbine i that are not blocked. Similar to BD_i, IBD_i can be considered to be a weighted average of the reciprocal of the distances to upstream blocking turbines, weighted by the fraction of areas blocked.

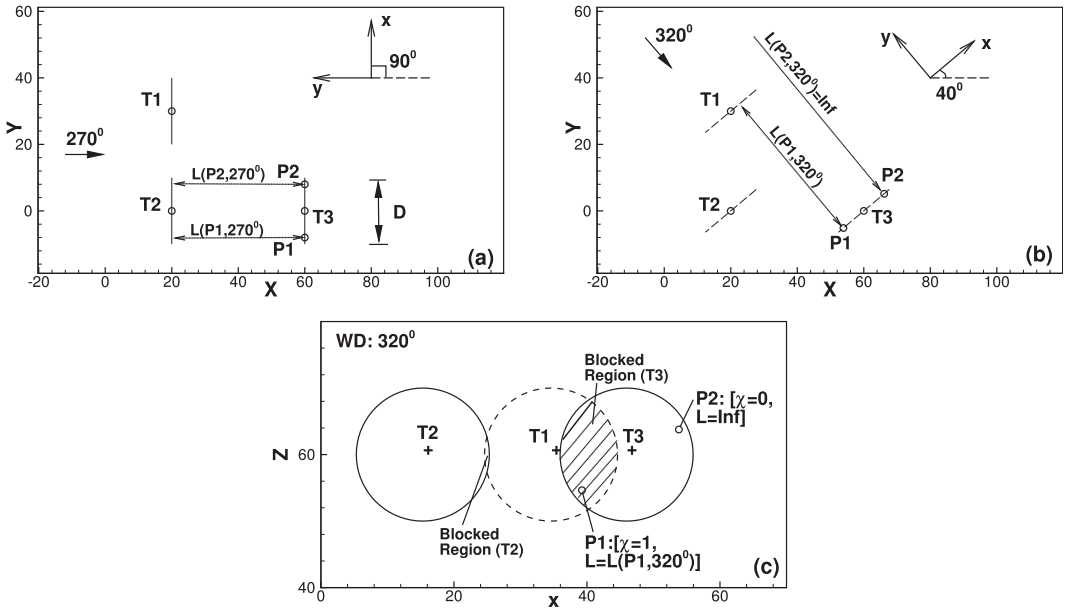

FIG. 2. Illustration of geometric measures in a simple three-turbine layout. Plan view with wind from (a) 270° and (b) 320°. (c) View from the rotated plane x–Z with the wind coming from 320°.

Also, IBD_i is not entirely independent of BR_i because the function χ is embedded in both definitions. IBD_i can be normalized by multiplying it by L_∞.

The fourth quantity, *blockage distance without weight* DNW_i, is simply the distance to the closest upstream turbine that blocks the swept area of turbine i, without any weighting by the fraction blocked. It can be defined formally as a minimum over all points on the swept area of turbine i, as

$$\mathrm{DNW}_i = \min_{(x,y)\in A}\{L, L_\infty\}, \tag{5}$$

where the quantity in the curly braces is defined for each point (x, y). As with BD_i, a turbine that is completely unobstructed is assigned the arbitrary value of L_∞, which is set to be $20D$ in this study. Unlike BD_i and IBD_i, this measure is truly independent of the blockage ratio.

The fifth quantity is *inverse blockage distance without weight* IDNW_i, which is the inverse of the distance to the closest upstream blocking turbine without weightage by the blockage fraction:

$$\mathrm{IDNW}_i = \frac{1}{\min_{(x,y)\in A}\{L\}}, \tag{6}$$

where L is defined above. Note that the definition of IDNW_i does not contain any arbitrary length and that, similar to DNW_i, IDNW_i is independent of the blockage ratio.

A simple three-turbine wind farm, shown in Fig. 2, is used as an example to illustrate the five geometric measures. Plan views of the layout are shown in Figs. 2a and 2b, with the wind directed along 270° and 320°, respectively. The (X, Y) coordinates of the three turbines are (20, 30) for T1, (20, 0) for T2, and (60, 0) for T3. These locations are marked with circles. The diameters of the turbines are 20 units each. The swept areas of the turbines are seen as solid lines in Fig. 2a and as dashed lines in Fig. 2b. It is assumed that the turbine yaw angle changes with the wind direction so that the swept area is always perpendicular to the incoming wind. A rotated coordinate system, x–y, attached to the turbine rotor disks, also changes with the wind direction. As a consequence, x makes an angle of 90° with the positive X axis in Fig. 2a and an angle of 40° with the positive X axis in Fig. 2b. Figure 2c shows the wind farm from the x–Z plane, when the wind is directed along 320°. The turbine rotor disks are perfect circles in this plane and overlap with each other. The overlap areas are marked in Fig. 2c.

With the wind blowing in the direction of the positive X axis—that is, $\theta = 270°$—the turbine swept areas are represented by the solid lines in Fig. 2a. For this configuration, there are no turbines upstream of T1 and T2, and, consequently, $\mathrm{BR}_1 = \mathrm{BR}_2 = 0$. Turbine T3 is completely blocked by T2, and hence $\mathrm{BR}_3 = 1$. Quantities BD_i and DNW_i are both equal to $20D$ for turbines T1 and T2 and are equal to the length $L(\mathrm{P1}, 270°)$ marked in Fig. 2a for turbine T3. Quantities IBD_i and IDNW_i are zero for T1 and T2 and are $1/L(\mathrm{P1}, 270°)$ for T3. When the wind direction changes to $\theta = 320°$, T1 remains unblocked ($\mathrm{BR}_1 = 0$), a tiny portion of T2 is

blocked by T1 (BR_2 is nonzero), and a large portion of T3 is blocked by T1 ($BR_3 \neq 1$). For this wind direction, the values of the four geometric measures remain unchanged from the 270° wind direction values for turbine T1. For turbine T3, the DNW_i and $IDNW_i$ will be $L(\mathrm{P1}, 320°)$ and $1/L(\mathrm{P1}, 320°)$, respectively, as marked in Fig. 2b. Terms BD_i and IBD_i will be weighted averages involving $L(\mathrm{P1}, 320°)$, L_{arb}, and their reciprocals, and with the blocked and unblocked areas as weights. Similarly, the geometric measures for turbine T2 with the wind directed along 320° will be different from the values with the wind along 270°.

To illustrate the two quantities χ and $Ł$, consider two points P1 and P2, marked by circles on turbine T3. When the wind is directed along 270°, point P1 on turbine T3 is blocked by turbine T2 and has $\chi = 1$; the distance to T2, $L(\mathrm{P1}, 270°)$, is shown in Fig. 2a. If the wind is directed along 320° (Figs. 2b,c), P1 is blocked by turbine T1. In this case, $\chi = 1$ again, but $L(\mathrm{P1}, 320°)$ now changes to the distance to T1. The other point P2 is blocked by turbine T2 when $\theta = 270°$, and $L(\mathrm{P2}, 270°)$ is identical to $L(\mathrm{P1}, 270°)$. With $\theta = 320°$, P2 is unblocked ($\chi = 0$). As a result, the distance $L(\mathrm{P2}, 320°)$ is infinite, and the arbitrary L_∞ needs to be introduced in Eqs. (3) and (5).

A Fortran 90 code was written to compute the five geometric measures, given a layout and a wind direction. The swept area of each turbine is divided into a large number (on the order of 1 million) of discrete areas. The quantities χ and L are computed at the geometric center of each discrete area, and the integrals in Eqs. (2)–(6) are evaluated numerically to give the geometric measures. The computation time is dependent almost entirely on the number of turbines and was about 1 min for each of the 80-turbine layouts evaluated in section 4. To evaluate the large number of layouts in a reasonable amount of time, multiple instances of the code were launched simultaneously, with each instance evaluating its subset of layouts, independent of others. Another Fortran 90 program was written for concatenating the results of different layouts and for postprocessing the raw data.

c. *Construction of geometry-based models*

The aim of this study is to develop geometry-based models of the form

$$P/P_{\max} = f(\mathrm{BR}, \mathrm{BD}, \ldots) \tag{7}$$

based on data from the eight LES simulations described earlier. Each individual turbine in each of the eight simulations constitutes one data point, giving a total of 278 data points (sum of column N_T in Table 1), which can be used for computing statistical averages.

TABLE 2. Correlation coefficients ρ of geometric measures Q with relative power $P/P_{\max}$ extracted from LES of the Lillgrund wind farm [$\rho(P/P_{\max}, Q)$].

Q	With front turbines	Without front turbines
BR	−0.8903	−0.9358
BD	0.8172	0.8633
IBD	−0.8127	−0.8549
DNW	0.5621	0.6831
IDNW	−0.3964	−0.5030

We begin by examining the correlations of the relative power $P/P_{\max}$, with the five directional measures individually. The correlation coefficient between two quantities a and b is defined as

$$\rho(a,b) = \frac{\langle ab\rangle - \langle a\rangle\langle b\rangle}{[(\langle a^2\rangle - \langle a\rangle^2)(\langle b^2\rangle - \langle b\rangle^2)]^{0.5}}, \tag{8}$$

where the angle brackets indicate ensemble averages (i.e., averages over the 278 data points available). It should be recalled that $\rho = \pm 1$ indicates perfect (positive or negative) correlation and that $\rho = 0$ indicates no correlation between a and b. Since $\rho(a, b) = -\rho(a, -b)$, for the purpose of determining whether two quantities correlate well with each other it is sufficient to look only at the magnitude of the correlation between them, without regard to its sign.

The second column in Table 2 shows that the blockage ratio has the highest correlation among all five measures, with a correlation-coefficient magnitude of 0.89. The two weighted distance measures, blockage distance and inverse blockage distance, are much better correlated with relative power than are the other two distance measures without weight.

For each wind farm layout, there are a few turbines that have a blockage ratio equal to zero. Depending on the wind direction, these turbines may or may not be located exclusively in the front row of the wind farm. Indeed, a front row can be identified only when the wind direction is perfectly aligned with the rows or columns—for example, 225° for Lillgrund. For all other layouts with rows/columns that are not perfectly aligned with the wind, it is impossible to identify unequivocally the front row. To avoid such ambiguity for layouts with arbitrary wind orientations, we refer to turbines with $BR_i = 0$ as "front row" turbines, even though in a few cases such turbines may actually be in the interior or at the edges of the wind farm.

Since these front-row turbines are not blocked by any upstream turbines, it is assumed that they encounter the undisturbed wind and generate the maximum power, which does not need to be modeled. We assign a relative

TABLE 3. Geometry-based models for $P_i/P_{\max}$ in terms of geometric measures, based on linear regression of data from LES of the Lillgrund wind farm.

Independent variable(s)	With front turbines		Without front turbines	
	Model	$\rho(P_i/P_{\max}, f)$	Model	$\rho(P_i/P_{\max}, f)$
BR_i	$f_1 = 0.858 - 0.417BR_i$	0.8903	$f_4 = \begin{cases} 0.872 - 0.430BR_i, & BR_i \neq 0 \\ 1, & BR_i = 0 \end{cases}$	0.9358
BR_i, BD_i	$f_2 = 0.667 - 0.318BR_i + 0.197BD_i/L_\infty$	0.9018	$f_5 = \begin{cases} 0.682 - 0.341BR_i + 0.213BD_i/L_\infty, & BR_i \neq 0 \\ 1, & BR_i = 0 \end{cases}$	0.9635
BR_i, IBD_i	$f_3 = 0.863 - 0.315BR_i - 0.038IBD_iL_\infty$	0.9043	$f_6 = \begin{cases} 0.894 - 0.338BR_i - 0.0405IBD_iL_\infty, & BR_i \neq 0 \\ 1, & BR_i = 0 \end{cases}$	0.9650

power of 1 to these front-row turbines and only model those turbines for which $BR_i \neq 0$. To evaluate the effectiveness of such a modeling strategy, the third column in Table 2 shows correlation coefficients between the relative power and the five geometric measures, with $P/P_{\max}$ enforced to be 1 for all data points that have $BR_i = 0$. The turbines with $BR_i = 0$ are, in a sense, excluded from the modeling, and we term this strategy as one with ''front turbines excluded.'' With the front turbines excluded, again the relative power is best correlated with the blockage ratio ($|\rho| = 0.94$), and the blockage distance and inverse blockage distance are better than the other two distances. We further note that the correlations in the third column are consistently better than those in the second column, which indicates that a strategy of modeling only those turbines that have $BR_i \neq 0$ is likely to be better than a strategy of modeling all turbines.

The inverse correlation of the relative power generated by a turbine with its blockage ratio, characterized by a negative ρ, appears to be intuitively correct. A turbine whose swept area is blocked by upstream turbines to a lesser extent (smaller BR_i) produces more power than a turbine that is heavily blocked (larger BR_i). Furthermore, while the magnitudes of these correlations are consistently high (larger than 0.89), it would be logical to expect that the blockage ratio is an incomplete measure of the wind farm, since it does not include any information about the length scales available for the wakes behind turbines to diffuse and dissipate and for the velocity profile to recover its original shape.

Motivated by these high correlations, we construct a total of six statistical models of the form

$$P_i/P_{\max} = f_m(BR_i, BD_i, \ldots), \quad m = 1, 2, 3, \ldots, 6, \tag{9}$$

as follows. A simple linear regression between the relative powers $P_i/P_{\max}$ and the blockage ratios BR_i with front-row turbine data included yields model $f_1(BR_i)$. A multiple linear regression with $P_i/P_{\max}$ as the dependent variable and BR_i and BD_i/L_∞ as the independent variables gives model $f_2(BR_i, BD_i)$. Similarly, model $f_3(BR_i, IBD_iL_\infty)$ is obtained by a multiple linear regression comprising BR_i and IBD_i. Similar linear regression analyses based on data with the front ($BR_i = 0$) turbines excluded yield models $f_4(BR_i)$, $f_5(BR_i, BD_i)$ and $f_6(BR_i, IBD_i)$. Note that the distance measures need to be nondimensionalized in order to combine them with the (nondimensional) blockage ratio.

The six models f_1–f_6 are listed in Table 3 along with the correlations between the actual and predicted relative powers $\rho(P_i/P_{\max}, f_m)$ for $m = 1, 2, 3, \ldots, 6$. All models show excellent correlations (larger than 0.89) with the relative powers obtained via LES. The models with front-row turbines excluded show even higher correlations, in excess of 0.95. As expected, the correlation coefficients $\rho(P_i/P_{\max}, f_1)$ and $\rho(P_i/P_{\max}, f_4)$ in Table 3 are identical in magnitude to the corresponding correlations listed for BR_i in Table 2. Furthermore, models based on a combination of BR_i with BD_i have higher correlations with the relative powers than do models based on BR_i alone. For example, $\rho(P_i/P_{\max}, f_2) > \rho(P_i/P_{\max}, f_1)$ and $\rho(P_i/P_{\max}, f_5) > \rho(P_i/P_{\max}, f_4)$. Similarly, models f_3 and f_6 are better correlated with $P_i/P_{\max}$ than are models f_1 and f_4, respectively. This indicates that the blockage ratio supplemented by one of the distance measures is a better indicator of the wind farm power.

Figure 3 shows the raw data from the LES simulations, marked by the different symbols, along with the fitting lines corresponding to functions f_1–f_6. In all of the subfigures shown, the high correlation between the LES results and the model predictions is apparent. Also, the numerous data points corresponding to $BR_i = 0$ in Figs. 3a–c collapse to a single point in Figs. 3d–f. As a result, the ''spread'' around the fitting line is smaller in these figures as compared with Figs. 3a–c. This is also reflected in the correlation coefficients accompanying the plots and listed in Table 2.

Models combining BR_i with the two nonweighted distance measures (DNW_i and $IDNW_i$) were also

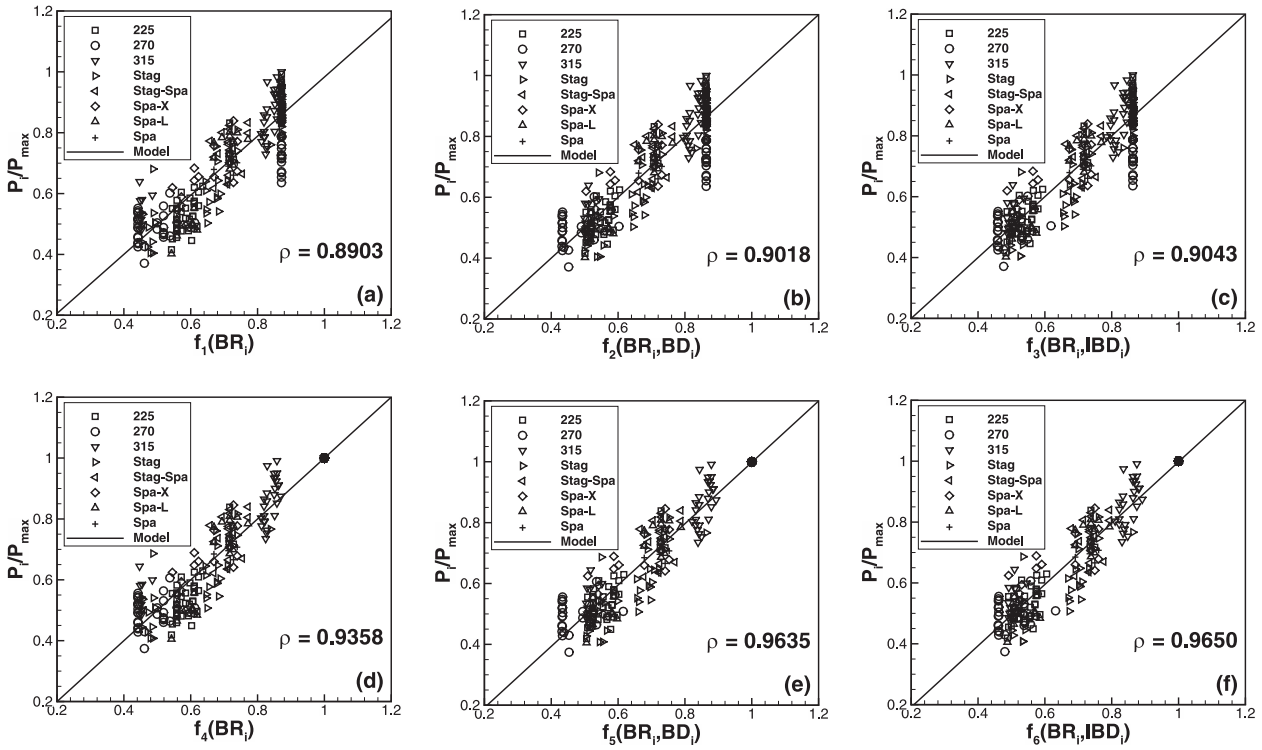

FIG. 3. Raw data (from neutral LES results) and linear regression fitting lines used in the construction of geometry-based models, with front-row turbines (a)–(c) included and (d)–(f) excluded.

investigated and were found to yield slightly smaller correlations than the models presented here in Table 3. For the sake of brevity, models based on DNW_i and $IDNW_i$ are not explored further in this paper. We also note that only linear models of geometric measures have been considered in this paper. Along similar lines, it may be possible to develop nonlinear models based on either linear or nonlinear combinations of the different geometric measures. In particular, the correlations with inverse distances suggest the use of hyperbolic functions. However, this is not pursued in this study in view of retaining simplicity and in view of the sufficiently high correlations obtained using linear models.

3. Validation of geometry-based models

The geometry-based models developed in the previous section are based on linear regression of data from LES of the Lillgrund wind farm. Before employing these models for general layout studies, they are evaluated for their ability to reproduce the results of LES and field observations in the Lillgrund and Horns Rev wind farm configurations.

a. Lillgrund wind farm

Any statistical model must, at a minimum, reproduce the data that went into building it. The geometry-based models developed are first validated by comparing their predictions for individual turbines with the LES data. Figure 4 compares the model predictions with the actual relative power obtained from the LES of the original Lillgrund layout, with the wind blowing from the southwest (case 225 in Table 1). Since the wind turbines in Lillgrund are aligned along southwest–northeast, it is natural to present the results for this wind direction along columns B–E as shown in Fig. 1a.

It is apparent that the geometry-based models capture the patterns of variability of turbine power along the columns very well. While there are underpredictions and overpredictions at some individual turbines, overall the model results compare very well to the LES results. Furthermore, the models with the front excluded (f_4–f_6; panels in the right column of Fig. 4) appear to be slightly more accurate than the models with front turbines included in their construction (f_1–f_3; panels in the left column of Fig. 4), as expected.

The ability of the models to reproduce field observations is evaluated next. As compared with predicting simulation data, reproducing observational data is a more rigorous test for the geometry-based models, because field observations invariably involve uncertainty regarding the wind speed, direction, and atmospheric stability conditions. For example, the observations at the

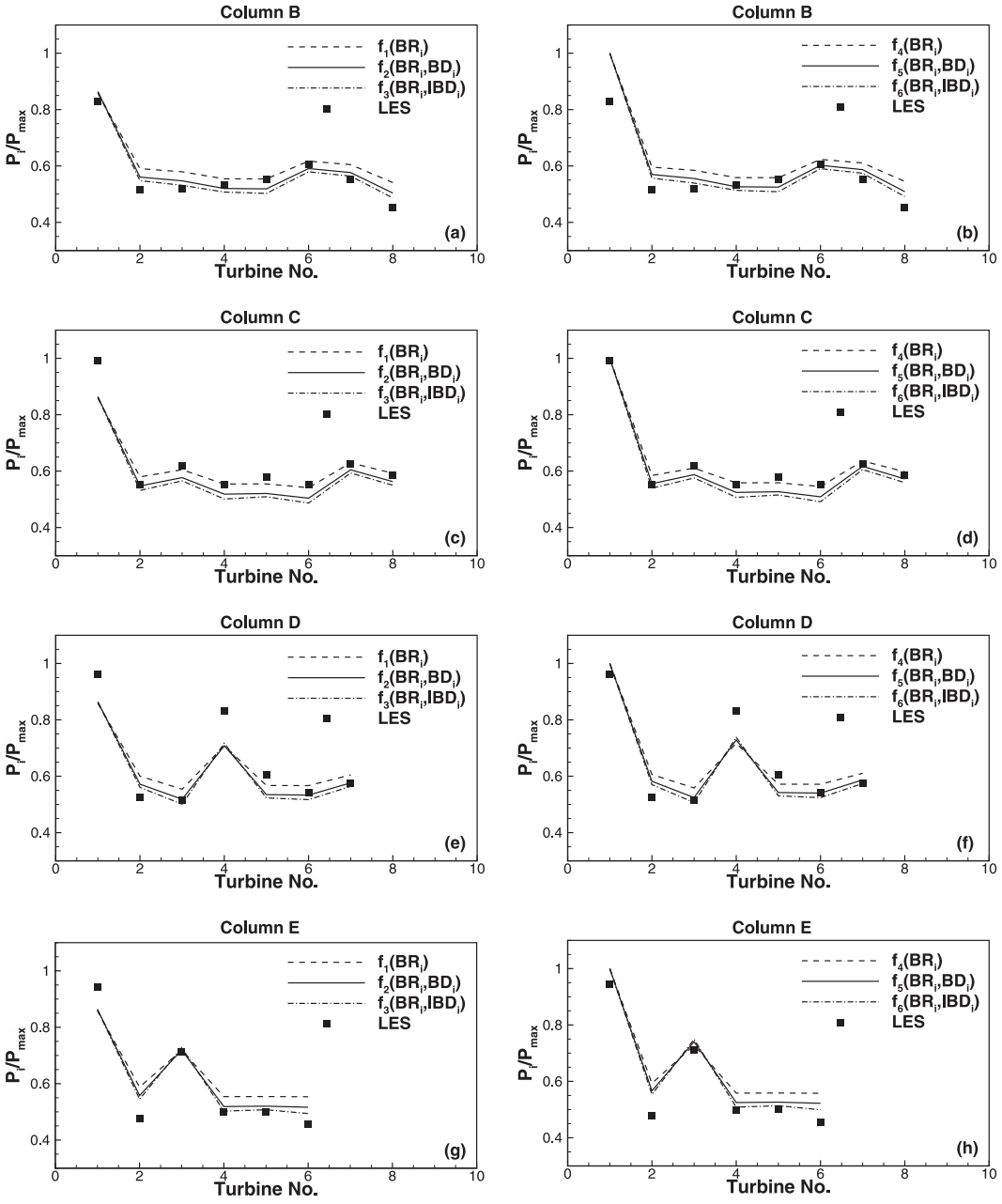

FIG. 4. Comparisons of relative power of turbines in the Lillgrund wind farm along columns (a),(b) B; (c),(d) C; (e),(f) D; and (g),(h) E for models based on LES data with front-row turbines (left) included and (right) excluded. LES results were reported by Archer et al. (2013).

Lillgrund wind farm reported in Dahlberg (2009) are averaged over several years and include different wind speeds. Most significant is that the observations lack information regarding atmospheric stability. It is thus likely that the averaged profiles obtained from observations include various stability conditions and cannot be reproduced precisely by models trained on data from well-controlled numerical simulations under neutral stability.

The power generated by turbine C2, normalized by the power generated by turbine C1 (see Fig. 1a for their positions), as predicted by several models, is compared in Fig. 5a with the observations reported in Dahlberg (2009). Wind directions varying from 200° to 240° are considered. Figure 5a shows that the geometry-based models overpredict $P(C_2)/P(C_1)$ over most angles. The overprediction is larger for wind directions in the vicinity

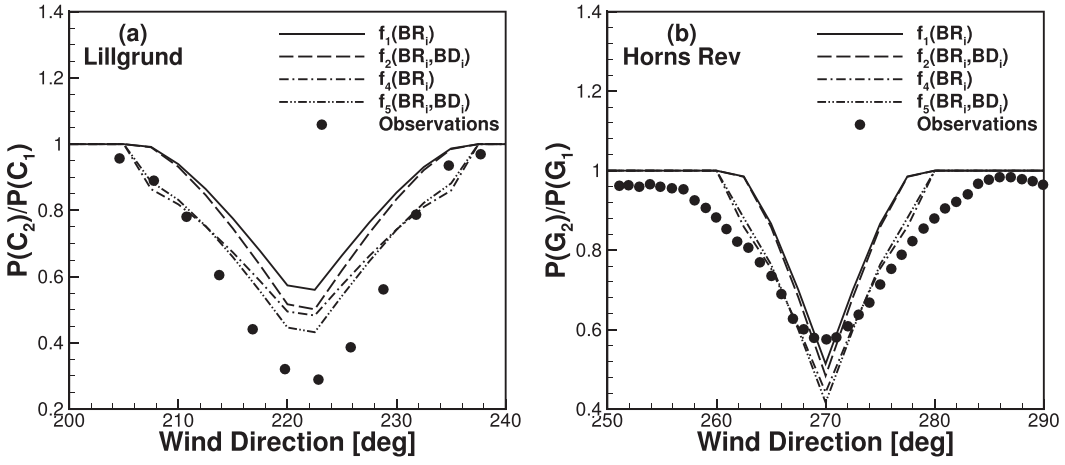

FIG. 5. Comparisons of (a) power of turbine C2 normalized by power of turbine C1 in the Lillgrund wind farm for various wind directions with field observations reported in Dahlberg (2009) and (b) power of turbine G2 normalized by power of turbine G1 in the Horns Rev wind farm for various wind directions with field observations reported in Hansen et al. (2012).

of 220°. Nevertheless, the overall shape of the profile is preserved. Also, as before, models with the front-row turbines excluded (f_4 and f_5) are more accurate than the models that include front-row turbines (f_1 and f_2).

Figure 6 plots the average relative power P_{rel} reported in Table 1 against the farm-averaged blockage ratio. The figure is composed of eight data points, one corresponding to each of the LES cases. Although the number of data points is limited, these global quantities can be seen to be almost perfectly correlated, with $\rho \approx -1$. The correlations between P_{rel} and the global averages of the independent variables corresponding to the other five geometry-based models have also been examined, and they too are found to be consistently and significantly higher than the correlations based on individual turbines. This indicates that these geometry-based models are likely to predict the global average power generated by a wind farm much more accurately than the power generated by individual turbines.

Over the eight LES cases, the farm-averaged power predictions of models f_4 and f_5 are found to have a bias error of approximately −6% and an rms error of approximately 4%. The negative value for the bias error indicates that these models underpredict the farm-averaged power by about 6% on average. The rms error provides a threshold value that can be useful while evaluating different layouts (see section 5). A comparison between two layouts can be considered meaningful only if the predicted powers differ by more than 4%.

b. *Horns Rev wind farm*

The performance of the geometry-based models is next assessed for a layout other than that of the Lillgrund wind farm. The Horns Rev wind farm, located in the North Sea off the coast of Denmark, comprises 80 turbines arranged in an almost rectangular layout of 10 numbered rows and eight lettered columns (Hansen et al. 2012; Gaumond et al. 2012). Figure 5b shows the power generated by turbine G2 over that of turbine G1 as a function of wind direction. The geometry-based model predictions are compared with field observations reported in Hansen et al. (2012), where the turbines are referred to as 17 and 7, respectively. The geometry-based models capture the overall trend; that is, the

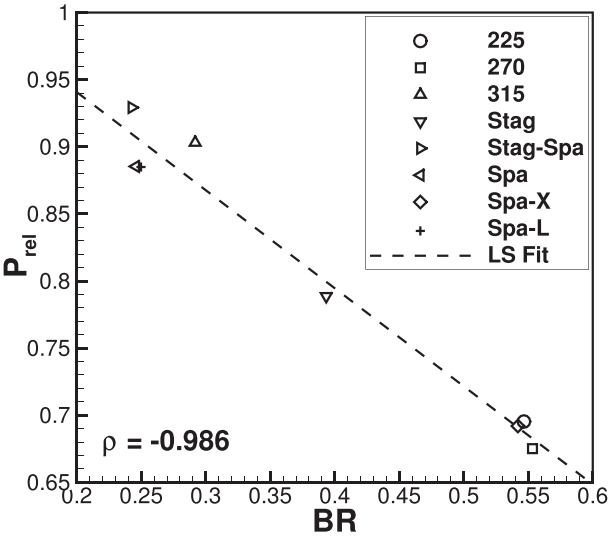

FIG. 6. Farm-averaged relative power as a function of farm-averaged blockage ratio, from the LES results. Fitting line and correlation coefficient is also shown.

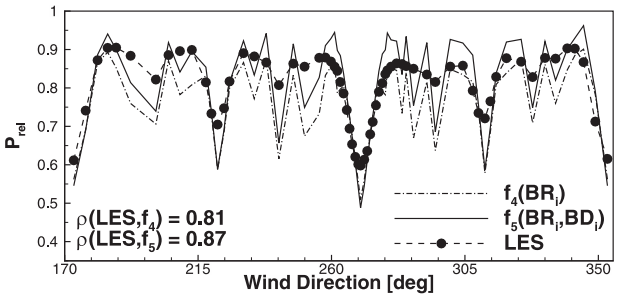

FIG. 7. Farm-averaged relative power as a function of wind direction in the Horns Rev wind farm, obtained from the geometry-based models and from LES reported in Porté-Agel et al. (2013).

power is reduced in the vicinity of 270°. However, it can be seen that the power is underpredicted on either side near 270° and overpredicted elsewhere. Recall, however, that, while the geometry-based models may not predict the power generated by individual turbines accurately, they are expected to be much more accurate for the farm-averaged quantities.

The relative power generated by the Horns Rev wind farm under different wind directions, as given by an LES study by Porté-Agel et al. (2013), is compared with geometric model predictions in Fig. 7. These LES simulations assumed a velocity of $8\,\mathrm{m\,s^{-1}}$ and a turbulence intensity of 7.7% at hub height (Porté-Agel et al. 2013). Predictions of f_4 and f_5 are shown in Fig. 7. As expected, the prediction of the farm-averaged relative power is more accurate than the prediction of the individual turbines seen in Fig. 5b. All the major trends in the LES results are reproduced by the two models. The magnitudes of relative powers are also captured reasonably accurately, although the geometry-based models display more variability than the LES results. Model f_5, based on the weighted distance BD_i, displays some overshoots and undershoots, while f_4, based on simply the blockage ratio mainly underpredicts the relative power. The LES results and the model predictions are well correlated, with coefficients 0.81 for $f_4(\mathrm{BR}_i)$ and 0.87 for $f_5(\mathrm{BR}_i, \mathrm{BD}_i)$. The improvement in the relative power prediction offered by f_5 over f_4 also demonstrates the contribution of the distance measure BD_i over and above that of the blockage ratio BR_i. Overall, the geometry-based models predict the relative power with 80%–90% accuracy. Figure 7 also demonstrates the power of geometry-based models, since the broad features of the LES results are generated at a fraction of the cost associated with the LES.

c. *Translating geometry-based models to other conditions*

The applicability of geometry-based statistical models trained on one set of data (LES of the Lillgrund wind farm, in this case) to other conditions is considered here. The power generated by a wind farm can be thought to depend on six parameters: the number and type of turbines, turbine layout, wind speed, atmospheric TI, and atmospheric stability. Section 3b showed that the models trained on LES of Lillgrund translated well to LES of Horns Rev. The two farms differed in the first four parameters, that is, number, type and layout of turbines, and wind speeds ($8.7\,\mathrm{m\,s^{-1}}$ in Lillgrund vs $8\,\mathrm{m\,s^{-1}}$ in Horns Rev at their respective hub heights). Both sets of LES were conducted under neutral stability and had similar levels of incoming turbulence intensities (7.3% in Lillgrund and 7.7% in Horns Rev at hub height). This indicates that the geometry-based models are able to account for differences in the first four parameters, as long as the last two are fixed.

The dependence on TI and atmospheric stability needs to be built into the geometry-based models. We anticipate that the correlations between the relative powers and the geometric quantities will still hold under different TI and stability conditions, albeit with different coefficients for the fitting functions. This issue will be considered in future studies.

It is always challenging to compare model predictions with field observations. First, field observations are often averaged over large periods of time; for example, the data in Dahlberg (2009) are averaged over a 2-yr period and therefore include flow conditions with widely varying TI and atmospheric stability levels. Furthermore, it is difficult to isolate conditions that match a few given criteria—for example, a certain wind speed at hub height—yet yield a sufficient number of measurements for meaningful averaging. Comparisons between model predictions of farm-averaged power data and field observations for different directions can only be carried out if good-quality observations are available and once the effects of TI and stability have been incorporated in the geometry-based models. For these reasons, we do not present comparisons with farm-averaged observations in this study.

In short, we conclude that geometry-based models calibrated on a few LES of a specific wind farm can reproduce the LES results of that wind farm, including different layouts and wind speeds, with a good level of accuracy. Furthermore, the geometry-based models can predict the farm-averaged power obtained from LES of other wind farms with reasonable accuracy. The models, however, cannot be assumed to translate well to wind farms operating under different levels of TI and stability or to reproduce field observations. In their present form, though, the geometry-based models can be used to study the effects of different design parameters under neutral conditions, and this is considered in the rest of the paper.

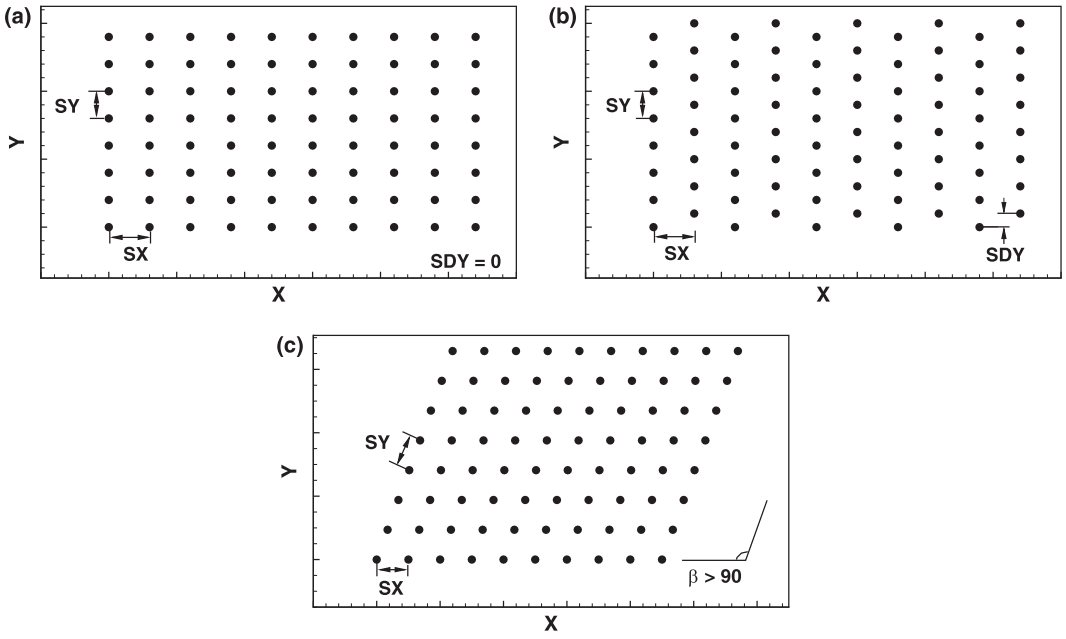

FIG. 8. Examples of wind farm layouts with different design variables. Solid circles represent individual turbines. (a) Rectangular layout without staggering of alternate rows, (b) rectangular layout with alternate rows staggered, and (c) rhomboidal layout, with nonorthogonal "rows" and "columns."

4. Evaluation of wind farm layouts using geometry-based models

The geometry-based models developed and evaluated above are used here to study the effects of wind turbine layout in a hypothetical wind farm comprising 80 turbines, arranged in 10 rows and eight columns, similar to Horns Rev. We introduce four design parameters, as shown in Fig. 8: the spacing SX between consecutive turbines in the X direction, the spacing SY between consecutive turbines in the Y direction, the staggering SDY of alternate rows in the Y direction, and the angle β between rows and columns. When $\beta = 90°$, the turbines are laid out in a regular rectangular grid and a rectangle bounding the entire layout can be identified easily (Fig. 8a), even when SDY $\neq 0$ (Fig. 8b). We term all layouts of the types shown in Figs. 8a,b as "rectangular." Layouts characterized by a bounding rhombus or a bounding diamond, as exemplified in Fig. 8c, are referred to as "nonrectangular," and the spacing between columns is denoted SY, although this is not exactly along the Y direction (Fig. 8c).

We first investigate a total of 420 rectangular layouts, constructed by varying SX in the range $[3D, 12D]$, SY over $[2D, 8D]$, and SDY over $[0, 5\text{SY}/6]$ in steps of D, D, and SY/6, respectively ($10 \times 7 \times 6 = 420$). In addition, 576 nonrectangular layouts are investigated in section 4d, with SX $\in [3D, 10D]$, SY $\in [3D, 10D]$, and $\beta \in [70°, 90°]$ in steps of D, D, and 5°, respectively. For each rectangular layout, 37 wind directions are assumed, with θ varying from 270° to 360° in steps of 2.5°. The range of wind directions is confined to only 90° since there is a four-way symmetry associated with rectangular layouts. Given a generic geometric measure $G(\theta)$, $\theta \in [270°, 360°]$, the measure for other wind angles can be determined using

$$G(\theta) = \begin{cases} G(360° - \theta), & \theta \in [0°, 90°] \\ G(180° + \theta), & \theta \in [90°, 180°] \\ G(540° - \theta), & \theta \in [180°, 270°]. \end{cases} \quad (10)$$

Similarly, each nonrectangular layout is combined with 73 wind directions in steps of 2.5° over the range [270°, 450°] (or, equivalent, $[-90°, 90°]$). This range is sufficient to cover all directions, since nonrectangular layouts display a two-way symmetry, and the geometric measures over the rest of the angles can be determined according to

$$G(\theta) = G(180° + \theta), \quad \theta \in [90°, 270°]. \quad (11)$$

The different wind directions considered here are assumed to be independent of each other. Keeping the farm layout fixed and varying the wind directions is equivalent to fixing the wind direction and rotating the entire layout. Thus, evaluating the effect of different wind directions, in effect, allows for a study of layouts

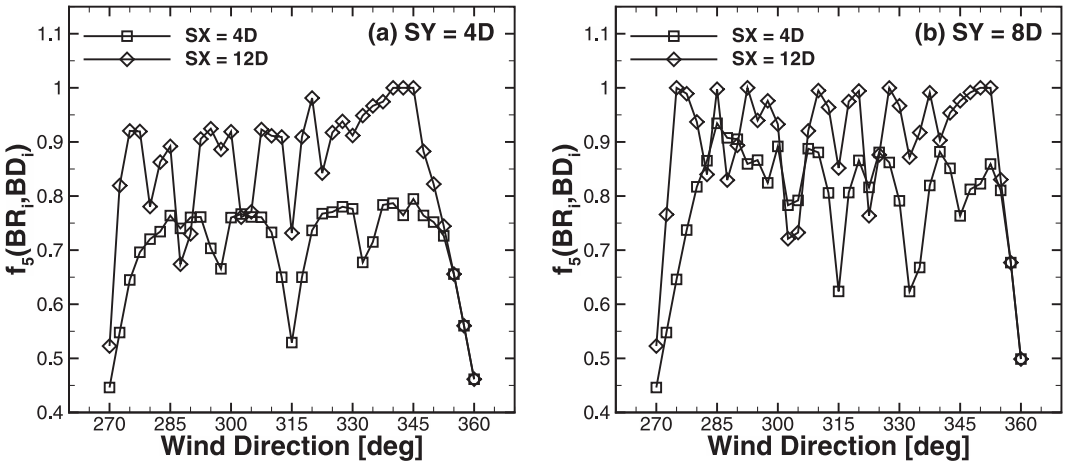

FIG. 9. Effect of wind direction on the relative power in a hypothetical wind farm with SDY = 0 and (a) SY = 4*D* and (b) SY = 8*D*.

with different orientations with respect to a fixed wind direction, for example, the prevailing one. Throughout this paper, we refer to wind directions and wind farm orientations interchangeably. The effect of frequency distributions of wind directions (described by wind roses) will be considered in a subsequent study.

For each layout and each wind direction, the three geometric measures for each turbine as well as the farm-averaged measures and the relative power predicted by the six models are evaluated. While it is impractical, and indeed unnecessary, to present all of the results, a few general observations and important trends are discussed below. The results of the six models are found to be very similar, and therefore only f_5 is discussed.

a. Effect of wind direction

The effect of wind direction on the power production in a nonstaggered wind farm is shown in Fig. 9. The results of four combinations of streamwise and spanwise spacings are shown. For all four combinations of spacings, the power production curves show local minima at $\theta = 270°$, 315°, and 360°. The first of these angles corresponds to the wind directed exactly along the columns. As a result, only the eight turbines at the extreme west of the wind farm are exposed to the undisturbed wind and all other turbines are completely shadowed ($BR_i = 1$) by these eight turbines, resulting in a very low value of the predicted power. Similarly, the other two angles correspond to the wind directed precisely along the rows and the diagonals of the wind farm, respectively, which again leads to $BR_i = 1$ for many of the turbines and results in small values of the predicted power.

Figure 9 further shows that the generated power increases drastically if the wind is slightly misaligned with respect to the three perfectly aligned directions discussed above. In all four curves, the power increases rapidly around $\theta = 270°$, 315°, and 360°. In comparing the curves with squares and diamonds in each panel, it is seen that the increase in power in the vicinity of 270° is much more dramatic if the spacing SX is larger. In the vicinity of 360°, however, the increase is dependent on the spacing SY rather than on SX.

The best offset angle at which the power curves display local maxima depends on the ratio S_{al}/S_{ac}, where S_{al} stands for spacing along the wind direction and S_{ac} stands for the spacing across the wind direction. Note here that the directions represented by the labels ''along'' and ''across'' vary with the wind direction. For example, with the wind directed along 270°, SX represents the spacing along the wind direction and SY represents the spacing across the wind direction. Conversely, with the wind directed along 360°, the labels are reversed, with SY and SX representing spacings along and across, respectively. For the curve for SX = 12*D* and SY = 4*D* (Fig. 9a), the local maximum in the vicinity of $\theta = 270°$ occurs for the offset $\Delta\theta = 5°$. In the vicinity of $\theta = 360°$, local maxima of power occur for $\Delta\theta = 15°$–20°. The values of the ratio S_{al}/S_{ac} for these two directions are 3 and ⅓, respectively. Similarly, for the curve for SX = 4*D* and SY = 8*D* (Fig. 9b), the local maxima of power in the vicinities of $\theta = 270°$ ($S_{al}/S_{ac} = ½$) and $\theta = 360°$ ($S_{al}/S_{ac} = 2$) occur at $\Delta\theta = 15°$ and 7.5°, respectively. This indicates the general trend that the best offset angle, with respect to a layout with rows or columns perfectly aligned with the wind direction, varies from approximately 15°–20° for smaller S_{al}/S_{ac} to around 5°–7.5° for larger values of S_{al}/S_{ac}.

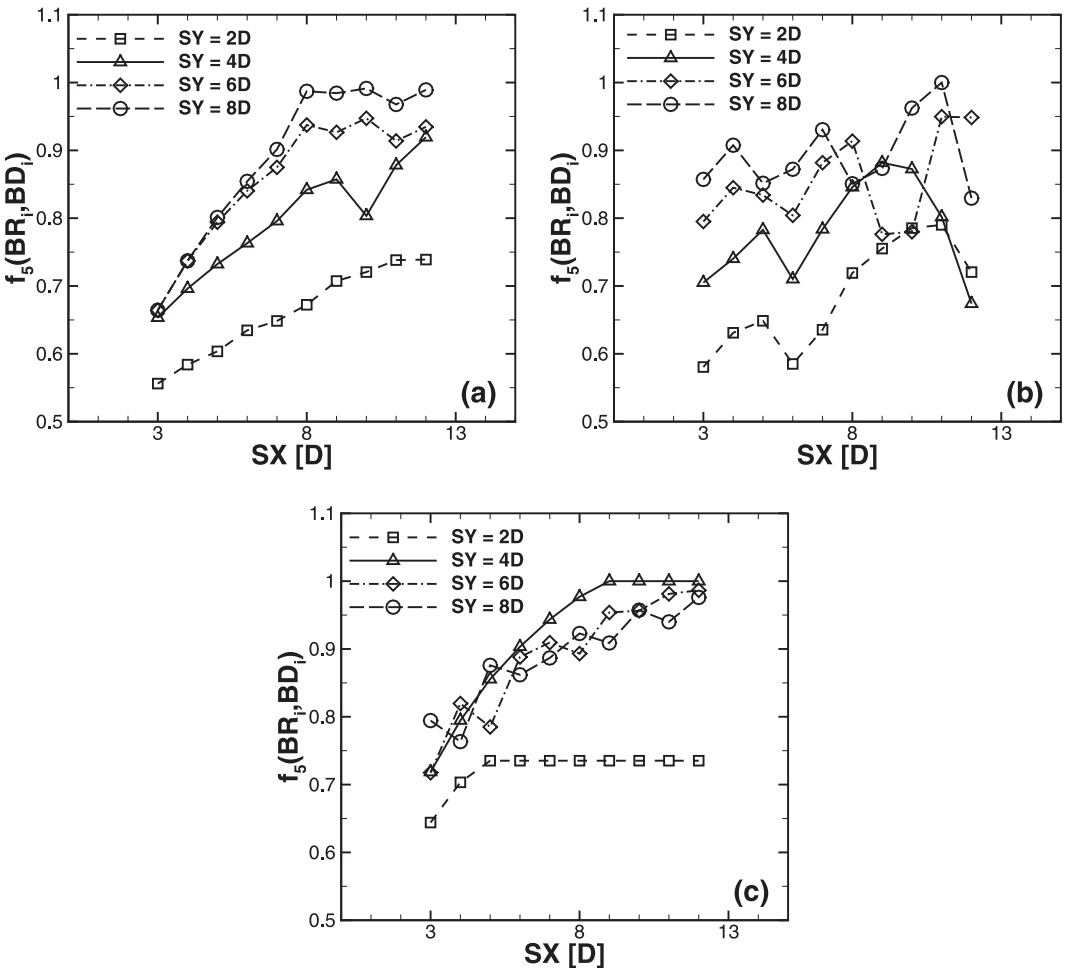

FIG. 10. Effect of axial spacing on the normalized power production in a hypothetical wind farm with SDY = 0, varying SY, and wind direction (a) 277.5°, (b) 287.5°, and (c) 345°.

These findings regarding the benefit of slight misalignment of rows of turbines with the wind direction are similar to those made by Stevens et al. (2014). The geometry-based models confirm that the findings made via LES of infinite arrays of turbines continue to hold for large, but finite, wind farms. The geometry-based models, however, incur a fraction of the computational cost of the LES of Stevens et al. (2014).

b. *Effect of turbine spacing*

From Fig. 9, the power with SX = 12*D* is smaller than that with SX = 4*D* in a few cases; for example, $\theta = 287.5°$ for SY = 4*D* and $\theta = 302.5° - 305°$ for SY = 8*D*. Thus, the general impression that larger spacing between turbines usually leads to smaller wake losses is found to be violated in a few stray cases. To examine this issue further, in Fig. 10 the variation of the power with the spacing SX is plotted for different values of SY without staggering, SDY = 0. Three wind directions are considered, corresponding to the offsets rated best according to Fig. 9.

With the wind directed along $\theta = 270° + 7.5°$, Fig. 10a shows that increasing SX leads to a more or less monotonic increase in the power prediction, for all SY. Figure 10b shows complicated interaction between SX and SY with the wind from $\theta = 270° + 17.5°$. For three of the four SY, the maximum spacing SX = 12*D* is found to be suboptimal. For SY = 4*D* and SY = 8*D*, the largest SX in fact yields the smallest power, smaller than even when SX is as small as 3*D*.

Looking at the effect of the spacing with the wind directed along the third of the optimal angles reported in Fig. 9—that is, $\theta = 345°$—the curves in Fig. 10c display the general trend of increasing power with increasing SX, followed by a saturation beyond a certain point. For SY = 12*D* the saturation is reached for SX as low as 5*D*, whereas for SY = 4*D* the power does not increase beyond SX = 9*D*. The power generated with SY = 6*D* and

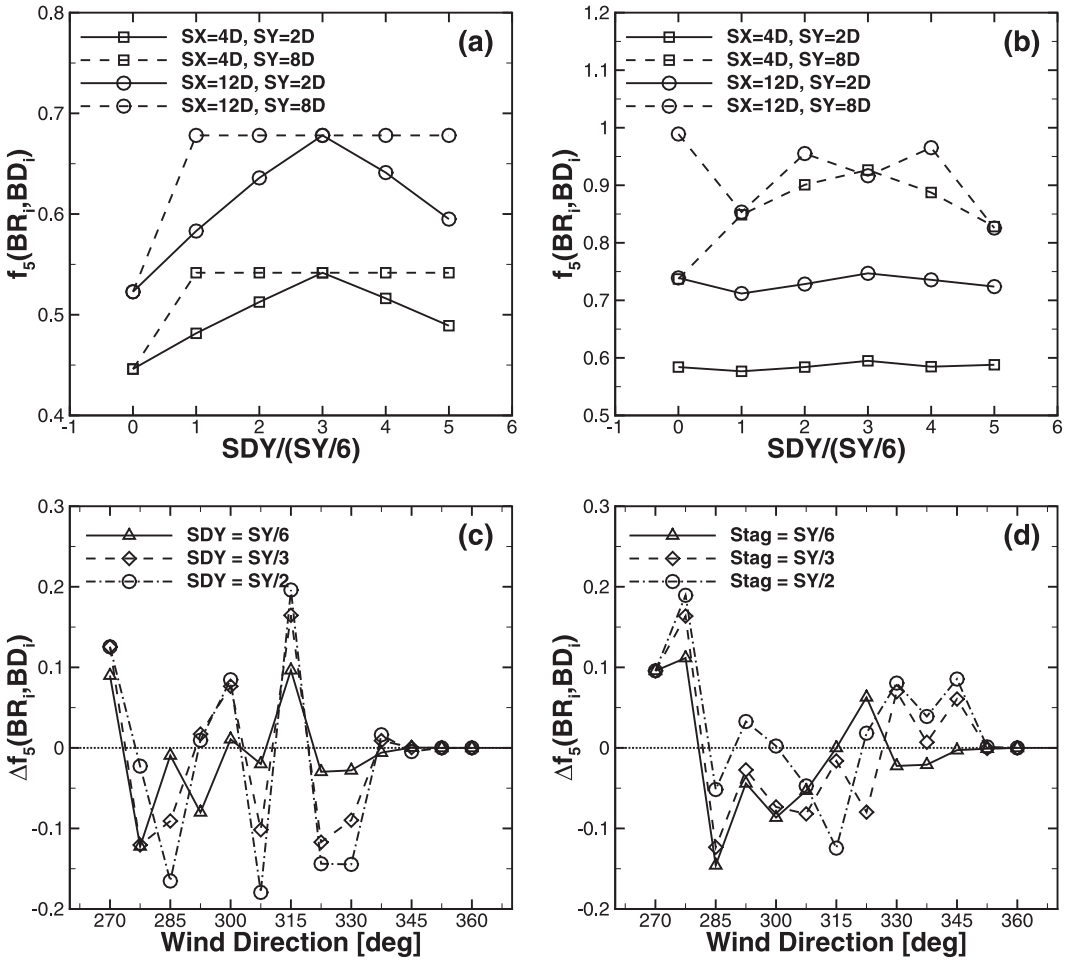

FIG. 11. Effect of staggering of alternate rows of turbines in a hypothetical wind farm for four combinations of axial and spanwise spacings, with the wind from (a) 270° and (b) 277.5°. Also shown is the change in the normalized power production due to staggering in a hypothetical wind farm for various wind directions and staggerings, and with (c) SX = 8*D* and SY = 4*D* and (d) SX = 4*D* and SY = 8*D*. SDY = 0 denotes the unstaggered configuration, and SDY = SY/2 denotes the perfectly staggered configuration.

SY = 8*D* does not saturate with increasing SX. Another striking observation in Fig. 10c is that for SX > 6*D* the power generated is maximum when SY = 4*D* and that for SX > 9*D* the model f_5 predicts zero wake losses when SY = 4*D*.

The reasons for the complicated interactions among SX, SY, and θ are purely geometric. Turbines that are not blocked by any upstream turbine in a layout with smaller spacing can, under certain wind directions, move into the shadow of an upstream turbine when the spacing is increased. Consequently, layouts with larger spacings produce less power than layouts with smaller spacings, in a few instances seen (Figs. 9, 10).

Although predictions of f_5 alone are shown in Fig. 10 (and all other figures in this section), the predictions of other models, particularly f_4, are qualitatively similar with slight quantitative differences.

c. *Effect of staggering of alternate rows*

The numerical simulations by Archer et al. (2013) showed that the power at Lillgrund increased by almost 33% over the perfectly aligned configuration when alternate rows were staggered. In that study, alternate rows were displaced by SDY = SY/2 to yield a configuration that may be termed "perfectly staggered." Figure 11 shows the effect of two additional steps between the perfectly aligned and perfectly staggered configurations (SDY = SY/6 and SDY = SY/3) and two steps beyond the perfectly staggered configuration (SDY = 4SY/6 and SDY = 5SY/6). Four different combinations of turbine spacings and two different wind directions are considered. With the wind directed along 270°, Fig. 11a shows that, for small values of SY (solid lines), the power first increases monotonically with

increasing SDY and that the perfectly staggered configuration yields the optimal power. The relative power prediction then decreases as staggering increases beyond SDY = SY/2. For larger values of SY (dashed lines), however, the optimum power is reached at SDY = SY/6, well before the perfectly staggered configuration. In other words, staggering of alternate rows is beneficial only up to the point at which the turbines in the second row step out of the shadow of the turbines in the first row. Increasing SDY beyond this point does not lead to an increase in power.

Figure 11b shows that the staggered configurations are not always beneficial as compared with the nonstaggered configurations when the wind is directed along $\theta = 270° + 7.5°$. Note that, irrespective of the wind direction, the staggering of alternate rows is always defined in the north–south direction along Y in this study. Figure 11b shows that different values of SDY yield the optimum power, depending on the turbine spacings SX and SY.

The advantage offered by configurations with nonzero SDY over configurations with SDY = 0, over all wind directions for two combinations of turbine spacings, is shown in Figs. 11c and 11d. The quantity plotted is $\Delta f_5 = f_5(\text{SDY} > 0) - f_5(\text{SDY} = 0)$. A complex interplay between the turbine spacings, staggering, and wind directions is seen. For example, with the wind directed along 315°, staggering is beneficial ($\Delta f_5 > 0$) in a wind farm with SX = 8D and SY = 4D but not beneficial in a wind farm with SX = 4D and SY = 8D. Staggering leads to increased power in both of these farms with the wind directed along 270°, but it leads to a reduction in power in both wind farms with the wind along 285°. Since the staggering is in the north–south direction, it has no effect on the power production when the wind is directed along 360°. Also, there might be instances in which intermediate staggering, SDY = SY/6 or SY/3, is preferable to perfect staggering, SDY = SY/2, for example, as seen in Fig. 11c for $\theta = 285°$ and in Fig. 11d for $\theta = 315°$.

In addition to two intermediate steps between the perfectly aligned and perfectly staggered configurations, layouts with SDY = 4SY/6 and SDY = 5SY/6 were also investigated. Figures 11a and 11b show that, as may be expected from geometry, the relative power predictions for layouts with SDY = 4SY/6 were found to be almost exactly equal to the relative power predictions for layouts with SDY = SY/3. Similarly, layout configurations with SDY = 5SY/6 were found to be almost identical to configurations with SDY = SY/6. This was found to hold for all combinations of spacings and wind directions examined. The staggered configurations, thus, show symmetry around the corresponding perfectly staggered (SDY = SY/2) configurations.

d. Nonrectangular layouts

The effect of changing β, the angle between the rows and the columns of the wind farms, is considered in this section. This angle was fixed to be $\beta = 90°$ in sections 4a–c. As explained earlier, orthogonal layouts involve a four-way symmetry whereas nonorthogonal layouts exhibit only two-way symmetry. Thus, in order to examine the influence of wind blowing over all directions, a sector of width 180° needs to be considered for nonorthogonal layouts, as opposed to a 90°-wide sector for orthogonal layouts. We consider the sector [270°, 450°], which may also be referred to as ranging over [−90°, 90°].

Figures 12a and 12b plot the changes in the power brought about by changing β to 70° and 110° for different wind directions. Two combinations of the spacings SX and SY are considered. The dotted line marks the zero level, corresponding to $\beta = 90°$ (rectangular layout). The power produced can either increase or decrease [$f_5 - f_5(\beta = 90°) > 0$ or < 0, respectively] in nonorthogonal layouts, in comparison with orthogonal layouts, depending on the wind direction. For both combinations of SX and SY considered, the largest benefit occurs for a wind direction around 360°, whereas there is no benefit as $\theta \to \pm 90°$. This is easily understood, since changing β to nonorthogonal values leads to an increase in the number of turbines directly encountering the undisturbed wind when the wind is along 360°, whereas the number of front-row turbines does not change for wind directions of ±90°.

The effect of β for one particular wind direction ($\theta = 315°$), fixed SY = 4D, and different SX is shown in Figs. 12c and 12d. For SX = 4D and SX = 8D, all of the nonorthogonal layouts evaluated are better than the orthogonal layout. This is seen in Fig. 12c as well as in Fig. 12d, which plots the difference between the power predicted and that predicted for the corresponding orthogonal ($\beta = 90°$) layout. For SX = 10D, however, most of the layouts generate less power as compared with the orthogonal layout. In particular, layouts with highly obtuse $\beta > 100°$ generate much less power as compared with layouts with $\beta \leq 95°$. This illustrates that the effect of β can be different for different turbine spacings.

e. Layouts with zero blockage ratio

Of the 15 540 combinations of rectangular layouts and wind directions evaluated in this section, 225 had a global blockage ratio equal to zero. In other words, in these configurations, none of the turbines' swept area was blocked by that of other upstream turbines. Evidently, all of the geometry-based models predicted very high values of power for these cases. It is instructive to examine these layouts more closely.

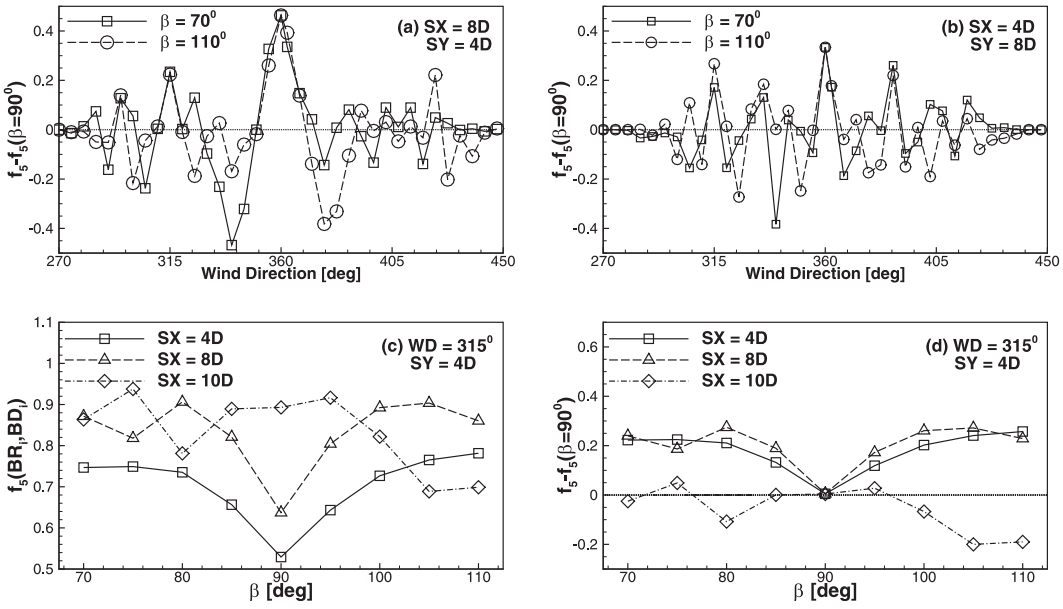

FIG. 12. Effect of nonorthogonal arrangement of rows and columns ($\beta \neq 90°$) in a hypothetical wind farm: The difference between the predictions of f_5 for $\beta \neq 90°$ and $\beta = 90°$ for varying wind directions and (a) SX = 8D and SY = 4D and (b) SX = 4D and SY = 8D. Also shown is the effect of β on (c) the power predicted and (d) the difference between the predicted power and that predicted for the corresponding orthogonal layout, for various SX and a fixed SY = 4D, with the wind directed along 315°.

All the layouts with BR = 0 had SX at least equal to 9D. The number of cases with BR = 0 increased with increasing SX. For SX = 9D, BR = 0 was found in only 15 cases, whereas the number of cases with BR = 0 increased to 96 when SX increased to 12D. For a given (sufficiently large) SX, layouts with BR = 0 were found for all values of SY—even as small as 2D or 3D. This indicates that wind farms that keep wake losses to very low values, while occupying very small areas, can be constructed by keeping spacing in one direction very small and making appropriate choices of the spacing in the other direction and of the alignment with the wind direction.

A few layouts that yield zero BR are shown in Fig. 13. The differences in the X and Y extents of different panels should be noted. As mentioned above, Figs. 13a and 13c have a very small SY = 3D, although the spacing SX = 9D is large. The wind directions for which zero BR is obtained are shown in each panel. For (SX, SY) = (9D, 3D) and for (SX, SY) = (9D, 8D), zero blockage is obtained for only one wind direction each. As the spacing SX increases, the sectors of wind directions for which zero blockage is obtained increase steadily. As shown in Figs. 13c and 13d, zero blockage ratios are obtained for 7.5°- and 5°-wide sectors for layouts with (SX, SY) = (12D, 3D) and (SX, SY) = (12D, 8D), respectively. Comparing Figs. 13a and 13c with Figs. 13b and 13d, respectively, it is seen that the effect of increasing spacing SY leads to a change in the wind direction that yields zero blockage. The width of the sector over which BR = 0 is only modestly affected by the changes in SY.

Note that in an actual wind farm the wind rarely blows from one fixed direction and can be described more accurately by considering a small sector centered around one direction. In view of this variability of the wind direction, layouts shown in Figs. 13c and 13d should be considered to be better than those in Figs. 13a and 13b. This is because the blockage is zero over small sectors of wind directions in the former set of layouts, as opposed to being zero for only a single wind direction in the latter. Layouts that offer zero blockage over a range of wind directions should be considered to be more robust than those that yield zero blockage for only a single wind direction.

A number of nonorthogonal layout–wind direction combinations also yield zero blockage, as long as the spacing in at least one direction is 9D or greater. A couple of nonorthogonal layouts and associated wind directions with BR = 0 are shown in Figs. 13e and 13f. As expected, the wind directions that yield zero blockage change with the angle β. One of the wind directions ($\theta = 347.5°$ for $\beta = 70°$ and $\theta = 372.5°$ for $\beta = 110°$), in each case, consistently makes an angle of 7.5° with the

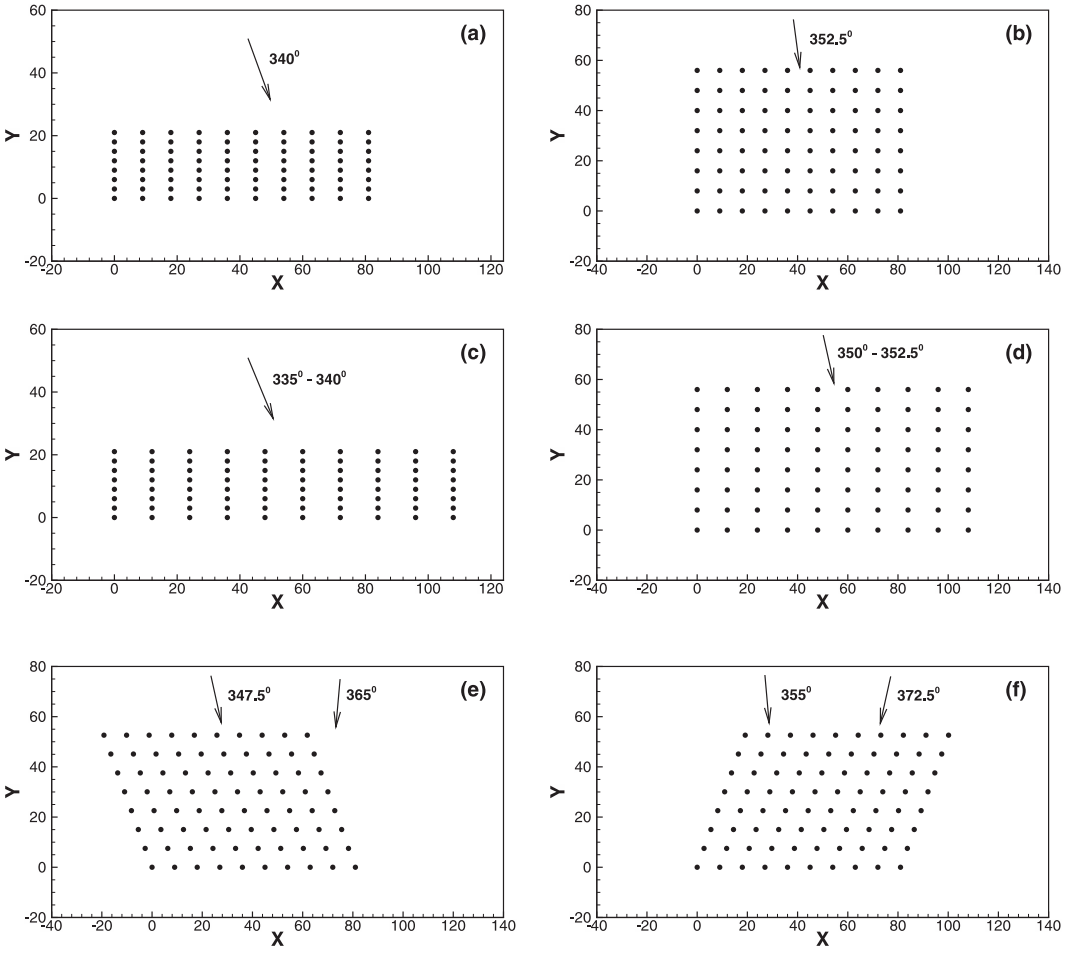

FIG. 13. Examples of layouts with global blockage ratio BR = 0. Arrows and labels indicate wind directions over which BR = 0. Rectangular layouts, $\beta = 90°$, with (a) SX = 9D and SY = 3D; (b) SX = 9D and SY = 8D; (c) SX = 12D and SY = 3D; and (d) SX = 12D and SY = 8D. Also shown are nonrectangular layouts with SX = 9D and SY = 8D and (e) $\beta = 70°$ and (f) $\beta = 110°$.

columns. The nonorthogonal layouts also exhibit a symmmetry with respect to the north–south direction. For example, the $\theta = 365°$ wind direction in the layout with $\beta = 70°$ is mirrored by the $\beta = 110°$ layout with the wind along $\theta = 355°$. We also mention without details that, similar to the orthogonal layout cases, the number of nonorthogonal layouts and the wind direction sector widths that yield zero blockage ratios increase with increasing spacings.

f. Discussion

The findings in section 4 point to the difficulty involved in formulating a good wind farm layout. The turbine spacings in the X and Y directions, the staggering of alternate rows in the Y direction, the angle β between the rows and the columns, and the wind farm orientation all interact in a complex manner to determine the wake losses in a wind farm. This study is restricted to wind farms that comprise a finite number of identical turbines and is based on neutral stability conditions at a single TI level.

One way of applying the results in this paper is to calculate averages of relative power, weighted by the wind direction frequency distributions given by wind roses, for each combination of SX, SY, β, and SDY. The appropriately weighted relative power can then be optimized over different combinations of the design parameters. Such a study involving combinations of different wind directions will be discussed in a subsequent paper. Even with the limitation of considering wind directions individually, a few general rules can be formulated for determining efficient wind farm layouts that reduce wake losses:

- The columns of the wind farm should make a small angle with the wind. The precise value of the angle that yields the maximum power can vary between 7.5°

and 15°, or even 20°, depending on the spacings between the columns.

- In general, the larger the spacing between turbines is, the higher is the power generation. However, the spacing along both the axes of the rectangular grid need not be large. If oriented correctly, wind farms with highly elongated rectangular layouts yield larger power than wind farms with square layouts.
- Staggering of alternate rows along one of the axes of the rectangle is beneficial if the wind is directed mostly perpendicular to the direction of staggering, as this serves to move the turbines out of the shadow of upstream turbines. However, for certain combinations of farm orientation with respect to the wind and the spacings, staggering may lead to turbines moving into the shadow of upstream turbines, resulting in less power.
- Depending on the orientation of the farm with respect to the wind, nonorthogonal layouts might yield greater power than orthogonal layouts by increasing the number of turbines that encounter the undisturbed wind. Changing the angle between rows and columns from orthogonal to nonorthogonal may not necessarily be beneficial.

These general principles have been derived for wind farms with a regular grid of turbines. The combinations of the four design variables considered here by no means cover the entire gamut of different layouts possible. The geometry-based models developed, however, are general and can be easily applied to other arbitrary layouts as well.

5. Summary and outlook

Wake effects in wind farms can lead to a significant reduction in the power produced as compared with the installed capacity in a wind farm. Hence, layout studies are critical components in the design of large wind farms. In contrast to analytical and CFD-based models, statistical models based on geometric quantities associated with the farm layout have been developed here. Results of large-eddy simulations of the Lillgrund wind farm, reported in Archer et al. (2013), are used for calibrating the models.

The basic idea is that the geometric blockage of wind turbine disks by other upwind turbines overwhelmingly controls the wake losses and the power generation. The geometric quantities that we term blockage ratio, blockage distance, and inverse blockage distance, and their linear combinations, are found to be very well correlated with the relative power generated by the turbines. The correlations between the relative power and the geometric measures are found to be even better (in excess of 0.95 in most cases), when the variables are averaged over the entire wind farm. Inspired by these high correlations, six simple models have been developed based on the geometric quantities and the Lillgrund LES results. Although all six models are of comparable accuracy, model f_5 may be considered to be the most complete, since it contains elements of the blockage ratio as well as the distance to the upstream blocking turbines.

The models are evaluated by comparison with observations and LES results of the Lillgrund and Horns Rev wind farms. It is shown that models trained on the results of LES of the Lillgrund wind farm translate reasonably well to other wind farms with the same stability and incoming turbulence intensity. In particular, the broad features of the LES results of the Horns Rev wind farm are reproduced to a reasonable level of accuracy. Comparisons with observations show that there may be some discrepancies between the model predictions and individual turbine power. However, the models are expected to be reasonably accurate with respect to prediction of the global, farm-averaged power. Comparisons with actually observed farm-averaged power values are difficult because the observations are averaged over long time periods, comprising effects of differing levels of turbulence intensity and atmospheric stability. Further work incorporating the effects of these parameters in the geometry-based models needs to be carried out in the future to perform effective and fair comparisons.

The geometry-based models are used to study different layouts in hypothetical wind farms, with turbines arranged in regular rectangular or rhomboidal layouts. A total of 15 540 rectangular combinations and approximately 42 000 nonrectangular combinations are obtained by varying the spacings in the X and Y directions, the staggering of alternate rows in one direction, the angle between the rows and the columns, and the orientation of the wind farms with respect to the wind direction. It is found that the optimum layout is a complicated and nonintuitive function of the different design parameters.

The orientation of the wind farm, defined as the angle between the columns and the prevailing wind direction, is found to be the most critical design parameter. This angle should be small, between 7° and 20°, but should not be zero, which would correspond to a perfectly aligned orientation and thus one with maximum losses. Small changes in this orientation angle can, in some cases, lead to drastic improvement or deterioriation in the generated power.

The spacing between turbines is another important design consideration. It is found that the spacing along at

least one direction should be fairly large (approximately $9D$ or more). The spacing along the other direction can be as small as $2D$ if the wind varies within a very narrow sector. Slightly larger spacings in this second direction can be used in order to account for the variability in the wind direction usually found in the field.

The effect of staggering alternate rows along one of the axes of the rectangle is found to depend heavily on the orientation of the wind farm with respect to the wind direction and can lead to significant increases or decreases of the generated power. The effect of the angle between the rows and the columns too is dependent largely on the farm orientation with respect to the wind.

In addition to the general principles outlined above, this study also demonstrates the advantages of the geometry-based models over other physics-based numerical simulation techniques. Using the geometry-based models, a large number of layouts can be evaluated at a fraction of the cost associated with CFD-based tools. An LES or RANS study covering a similar number of layouts is prohibitively expensive. The geometry-based models can be very useful when used in conjunction with high-resolution numerical simulations, since a large number of layouts can be screened very quickly with these models. As mentioned in section 3a, a criterion to select the subset of best layouts would be to include only those that increase the power production by 4% or more over a control layout. The details of a few near-optimal layouts so identified can then be investigated using high-resolution numerical simulations.

There are several limitations to the current study. This study does not aim at minimizing the levelized cost of electricity (LCOE), which is a more complete measure of farm performance. Minimizing the LCOE requires estimates of the lifetime of a wind farm and operation and maintenance costs, among other things, and is beyond the scope of the present study. Maximizing the power generated by minimizing the losses due to interactions among turbines is, nevertheless, an important step in achieving an optimal wind farm. This study is concerned with determining the optimal layout of turbines so as to minimize wake losses, without considering operation and maintenance costs.

Another limitation of the current work is the fact that only regular rectangular or rhomboidal layouts of wind turbines have been investigated. More complex and seemingly random turbine layouts can potentially be more efficient than the regular layouts examined here. The level of incoming atmospheric turbulence can also impact the spread of the turbine wakes, thus affecting the overall farm performance. The sensitivity of these models to the turbulence level will be investigated in the future. Furthermore, since TI is known to be affected directly by the atmospheric stability, future work also includes extension of the models to account for unstable and stable stratification. It is expected that the incorporation of these effects will also make possible accurate and fair comparisons with field observations. Evaluation of layouts under the influence of multiple wind directions (with wind distributions given by wind roses) and the incorporation of geometry-based models in advanced optimization algorithms will also be pursued in the future.

Acknowledgments. Partial support for this research was provided by the National Science Foundation (Grant 1357649). All simulations were conducted on the Mills High Performance Computer cluster of the University of Delaware.

REFERENCES

Archer, C. L., S. Mirzaeisefat, and S. Lee, 2013: Quantifying the sensitivity of wind farm performance to array layout options using large-eddy simulation. *Geophys. Res. Lett.*, **40**, 4963–4970, doi:10.1002/grl.50911.

——, and Coauthors, 2014: Meteorology for coastal/offshore wind energy in the United States: Recommendations and research needs for the next 10 years. *Bull. Amer. Meteor. Soc.*, **95**, 515–519, doi:10.1175/BAMS-D-13-00108.1.

Barthelmie, R. J., and Coauthors, 2009: Modelling and measuring flow and wind turbine wakes in large wind farms offshore. *Wind Energy*, **12**, 431–444, doi:10.1002/we.348.

Bastankhah, M., and F. Porté-Agel, 2014: A new analytical model for wind-turbine wakes. *Renewable Energy*, **70**, 116–123, doi:10.1016/j.renene.2014.01.002.

Bergström, H., 2009: Meteorological conditions at Lillgrund. Vattenfall Vindkraft AB 6_2 LG Pilot Rep., 25 pp. [Available online at http://corporate.vattenfall.se/globalassets/sverige/om-vattenfall/om-oss/var-verksamhet/vindkraft/lillgrund/meteorological_conditions.pdf.]

Calaf, M., C. Meneveau, and J. Meyers, 2010: Large eddy simulation study of fully developed wind-turbine array boundary layers. *Phys. Fluids*, **22**, 015110, doi:10.1063/1.3291077.

——, M. B. Parlange, and C. Meneveau, 2011: Large eddy simulation study of scalar transport in fully developed wind-turbine array boundary layers. *Phys. Fluids*, **23**, 126603, doi:10.1063/1.3663376.

Churchfield, M. J., S. Lee, J. Michalakes, and P. J. Moriarty, 2012a: A numerical study of the effects of atmospheric and wake turbulence on wind turbine dynamics. *J. Turbul.*, **13**, N14, doi:10.1080/14685248.2012.668191.

——, ——, P. J. Moriarty, L. A. Martinez, S. Leonardi, G. Vijaykumar, and J. G. Brasseur, 2012b: A large-eddy simulation of wind-plant aerodynamics. *Proc. 50th AIAA Aerospace Sciences Meeting Including the New Horizons Forum and Aerospace Exposition*, Nashville, TN, AIAA, AIAA 2012-0537. [Available online at http://arc.aiaa.org/doi/abs/10.2514/6.2012-537.]

Dahlberg, J., 2009: Assessment of the Lillgrund Windfarm: Power performance wake effects. Lillgrund Pilot Project Vattenfall Vindkraft AB 6_1 LG Pilot Rep., 28 pp. [Available online at http://corporate.vattenfall.se/globalassets/sverige/om-vattenfall/om-oss/var-verksamhet/vindkraft/lillgrund/assessment.pdf.]

Emeis, S., 2010: A simple analytical wind park model considering atmospheric stability. *Wind Energy*, **13**, 459–469, doi:10.1002/we.367.

——, and S. T. Frandsen, 1993: Reduction of horizontal wind speed reduction in a boundary layer with obstacles. *Bound.-Layer Meteor.*, **64**, 297–305, doi:10.1007/BF00708968.

Frandsen, S. T., 1992: On the wind speed reduction in the center of large clusters of wind turbines. *J. Wind Eng. Ind. Aerodyn.*, **39**, 251–265, doi:10.1016/0167-6105(92)90551-K.

——, R. J. Barthelmie, S. Pryor, O. Rathmann, S. Larsen, J. Højstrup, and M. Thøgersen, 2006: Analytical modelling of the wind speed deficit in large offshore wind farms. *Wind Energy*, **9**, 39–53, doi:10.1002/we.189.

Gaumond, M., P.-E. Réthoré, A. Bechmann, S. Ott, G. C. Larsen, A. Peña, and K. S. Hansen, 2012: Benchmarking of wind turbine wake models in large offshore windfarms. Poster, *The Science of Making Torque from Wind*, Oldenburg, Germany, European Academy of Wind Energy. [Available online at http://www.forwind.de/makingtorque/Posters/Poster_71.pdf.]

Hansen, K. S., R. J. Barthelmie, L. E. Jensen, and A. Sommer, 2012: The impact of turbulence intensity and atmospheric stability on power deficits due to wind turbine wakes at Horns Rev wind farm. *Wind Energy*, **15**, 183–196, doi:10.1002/we.512.

Jensen, N. O., 1983: A note on wind generator interaction. Risø National Laboratory Doc. Risø-M-2411, 16 pp. [Available at http://orbit.dtu.dk/fedora/objects/orbit:88807/datastreams/file_3494b4b2-1dae-4442-941a-f2e628673f31/content.].

Katic, I., J. Høstrup, and N. O. Jensen, 1986: A simple model for cluster efficiency. *Proceedings of EWEC '86; European Wind Energy Association Conference and Exhibition*, W. Palz and E. Sesto, Eds., Vol. 1, A. Raguzzi, 407–410. [Available online at http://orbit.dtu.dk/fedora/objects/orbit:66401/datastreams/file_f7da8eb2-e49c-4dc9-9ee5-72846f40ef34/content.]

Meneveau, C., 2012: The top-down model of wind farm boundary layers and its applications. *J. Turbul.*, **13**, N7, doi:10.1080/14685248.2012.663092.

Meyers, J., and C. Meneveau, 2012: Optimal turbine spacing in fully developed wind farm boundary layers. *Wind Energy*, **15**, 305–317, doi:10.1002/we.469.

Nygaard, N. G., 2014: Wakes in very large wind farms and the effect of neighbouring wind farms. *J. Phys.: Conf. Ser.*, **524**, 012162, doi:10.1088/1742-6596/524/1/012162.

Peña, A., and O. Rathmann, 2014: Atmospheric stability-dependent infinite wind-farm models and the wake-decay coefficient. *Wind Energy*, **17**, 1269–1285, doi:10.1002/we.1632.

——, P.-E. Réthoré, C. B. Hasager, and K. S. Hansen, 2013a: Results of wake simulations at the Horns Rev I and Lillgrund wind farms using the modified Park model. DTU Wind Energy E. Rep. 0026(EN), 41 pp. [Available online at http://orbit.dtu.dk/fedora/objects/orbit:124519/datastreams/file_0949139f-cd04-4f8b-9921-fcd296a430ff/content.]

——, ——, and O. Rathmann, 2013b: Modeling large offshore wind farms under different atmospheric stability regimes with the Park wake model. *Proc. Int. Conf. on Aerodynamics of Offshore Wind Energy Systems and Wakes (ICOWES2013)*, Lyngby, Denmark, DTU Wind Energy, 634–644. [Available online at http://orbit.dtu.dk/files/69832671/Modeling_large_offshore_wind_farms.pdf.]

Porté-Agel, F., Y.-T. Wu, and C.-H. Chen, 2013: A numerical study of the effects of wind direction on turbine wakes and power losses in a large wind farm. *Energies*, **6**, 5297–5313, doi:10.3390/en6105297.

Smagorinsky, J., 1963: General circulation experiments with the primitive equations. I. The basic experiment. *Mon. Wea. Rev.*, **91**, 99–164, doi:10.1175/1520-0493(1963)091<0099:GCEWTP>2.3.CO;2.

Stevens, R. J. A. M., D. F. Gayme, and C. Meneveau, 2014: Large eddy simulation studies of the effects of alignment and wind farm length. *J. Renewable Sustainable Energy*, **6**, 023105, doi:10.1063/1.4869568.

——, ——, and ——, 2015: Coupled wake boundary layer model of wind-farms. *J. Renewable Sustainable Energy*, **7**, 023115, doi:10.1063/1.4915287.

Tian, L. L., W. J. Zhu, W. Z. Shen, J. N. Sørensen, and N. Zhao, 2014: Investigation of modified AD/RANS models for wind turbine wake predictions in large wind farm. *J. Phys.: Conf. Ser.*, **524**, 012151, doi:10.1088/1742-6596/524/1/012151.

Wu, Y.-T., and F. Porté-Agel, 2011: Large-eddy simulation of wind-turbine wakes: Evaluation of turbine parameterisations. *Bound.-Layer Meteor.*, **138**, 345–366, doi:10.1007/s10546-010-9569-x.

——, and ——, 2013: Simulation of turbulent flow inside and above wind farms: Model validation and layout effects. *Bound.-Layer Meteor.*, **146**, 181–205, doi:10.1007/s10546-012-9757-y.

Xie, S., and C. L. Archer, 2015: Self-similarity and turbulence characteristics of wind turbine wakes via large-eddy simulation. *Wind Energy*, **18**, 1815–1838, doi:10.1002/we.1792.